Fusion Algorithm for Remote Sensing Images Based on Nonsubsampled Contourlet Transform

YANG Xiao-Hui[1]　　　　JIAO Li-Cheng[1]

Abstract　　Considering human visual system and characteristics of images, a novel image fusion strategy is presented for panchromatic high resolution image and multispectral image in nonsubsampled contourlet transform (NSCT) domain. The NSCT can give an asymptotic optimal representation of edges and contours in image by virtue of its characteristics of good multiresolution, shift-invariance, and high directionality. An intensity component addition strategy based on LHS transform is introduced into NSCT domain to preserve spatial resolution and color content. Experiments show that the fusion method proposed can improve spatial resolution and keep spectral information simultaneously, and that there are improvements both in visual effects and quantitative analysis compared with the traditional principle component analysis (PCA) method, intensity-hue-saturation (IHS) transform technique, wavelet transform weighted fusion method, corresponding wavelet transform-based fusion method, and contourlet transform-based fusion method.

Key words　　Image fusion, nonsubsampled contourlet transform (NSCT), LHS transform, intensity component addition

Image fusion is a process by combining two or more source images from different modalities or instruments into a single image with more information. The successful fusion is of great importance in many applications, such as remote sensing, computer vision, medical imaging, and so on. In the pixel level fusion, some generic requirements can be imposed on the fusion results[1]:

1) The fused image should preserve all relevant information contained in the source images as closely as possible.

2) The fused process should not introduce any artifacts or inconsistencies, which can distract or mislead the human observer, or any subsequent image processing steps.

3) In the fused image, irrelevant features and noise should be suppressed to a maximum extent.

Panchromatic (PAN) images of high spatial resolution can provide detailed geometric information, such as shapes, features, and structures of objects of the earth's surface. While multispectral (MS) images with usually lower resolution are used to obtain spectral information necessary for environmental applications. The different objects within images of high spectral resolution are easily identified. Data fusion methods aim to obtain the images with high spatial and spectral resolution, simultaneously. The PAN and MS remote sensing image fusion is different from other fusion applications, such as image fusion in military missions or computer-aided quality control. The specificity is to preserve the spectral information for subsequent classification of ground cover. The classical fusion methods are principle component analysis (PCA), intensity-hue-saturation (IHS) transform, etc. In recent years, with the development of wavelet transform theory and multiresolution analysis, two-dimensional separable wavelets have been widely used in image fusion and have achieved good results[2−4].

Thus, the fusion algorithms mentioned above can hardly make it by themselves. They usually cause some characteristic degradation, spectral loss, or color distortion. For example, the IHS transform can enhance texture information and spatial features of fused images, but suffers from much spectral distortion. The PCA method will lose some original spectral features in the process of principal component substitution. The wavelet transform (WT) can preserve spectral information efficiently but cannot express spatial characteristics well. Furthermore, the isotropic wavelets are scant of shift-invariance and multidirectionality and fail to provide an optimal expression of highly anisotropic edges and contours in images.

Image decomposition is an important link of image fusion and affects the information extraction quality, even the whole fusion quality. In recent years, along with the development and application of the wavelet theory, the favorable time-frequency localization to express local signal makes wavelet a candidate in multisensor image fusion. However, wavelet bases are isotropy and of limited directions and fail to represent high anisotropic edges and contours in images well. The MGA emerges, which comes from wavelet multiresolution, but beyond it. The MGA can take full advantage of the geometric regularity of image intrinsic structures and obtain the asymptotic optimal representation. As an MGA tool, the contourlet transform (CT) has the characteristics of localization, multidirection, and anisotropy[5]. The CT can give the asymptotic optimal representation of contours and has been applied in image fusion effectively. However, the CT is lack of shift-invariance and results in artifacts along the edges to some extend. The nonsubsampled contourlet transform (NSCT) is in virtue the nonsubsampled filter banks to meet the shift-invariance[6]. Therefore, the NSCT is more suitable for image fusion. To meet different application demands either for human visual or statistical performance, we propose a highly effective NSCT fusion algorithm. Experimental results clearly demonstrate the superiorities of this proposed method when compared with other fusion algorithms.

This paper discusses the fusion of multispectral and panchromatic remote sensing images. An NSCT-based panchromatic and multispectral image fusion method is presented after analyzing the basic principles of remote sensing image system and fusion purpose. The rest of this paper is organized as follows. Section 1 gives the NSCT of

images. Section 2 introduces a novel fusion algorithm based on NSCT and LHS transform, and discusses the fusion rules in detail and approximate NSCT coefficients, respectively. Section 3 reports about the fusion experiments tested on PAN and MS image sets using the proposed algorithm and some other traditional ones, followed by the subjective and objective evaluations based on them. Conclusions are drawn in Section 4.

1 Nonsubsampled contourlet transform of images

1.1 Contourlet transform

Do and Vetterli proposed a "true" two-dimensional transform called contourlet transform, which is based on nonseparable filter banks and provides an efficient directional multiresolution image representation. The CT expresses image by first applying a multiscale transform, followed by a local directional transform to gather the nearby basis functions at the same scale into linear structures. For example, the Laplacian pyramid (LP) is first used to capture the point discontinuities, and then followed by a direction filter banks (DFB) to link point discontinuities into linear structures. In particular, contourlets have elongate supports at various scales, directions, and aspect ratios. The contourlets satisfy anisotropy principle and can capture intrinsic geometric structure information of images and achieve better expression than discrete wavelet transform (DWT), especially for the edges and contours.

However, because of the downsampling and upsampling, the CT is lack of shift-invariance and results in ringing artifacts. However, the shift-invariance is desirable in image analysis applications, such as edge detection, contour characterization, image fusion, etc[7].

Especially, during the realization of the CT, the analysis filter banks and synthesis filter banks of LP decomposition are nonseparable bi-orthogonal filter banks with band width larger than $\pi/2$. Based on multisampled rate theory, downsample on filtered image may result in lowpass and highpass frequency aliasing. Therefore, the frequency aliasing affects lie in directional subbands, which comes from the highpass subbands filtered by DFB. The frequency aliasing will result in information in a direction to appear in different directional subbands at the same time. This must weaken the directional selectivity of contourlets.

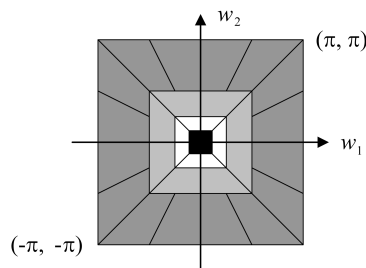## 1.2 Nonsubsampled contourlet transform

In order to get rid of the frequency aliasing of contourlets and enhance directional selectivity and shift-invariance, Cunha, Zhou, and Do proposed nonsubsampled contourlet transform based on nonsubsampled pyramid decomposition and nonsubsampled filter banks (NSFB)[6, 8]. The NSCT is the shift-invariant version of the CT and is built upon iterated nonseparable two-channel NSFB to obtain the shift-invariance. The NSCT provides not only multiresolution analysis but also geometric and directional representation.

Different from the CT, the multiresolution decomposition step of NSCT is realized by shift-invariant filter banks satisfying Bozout identical equation (Perfect reconstruction, PR) and not LP. Because of no downsample in pyramid decomposition, the lowpass subband has no frequency

aliasing, even the band width of lowpass filter is larger than $\pi/2$. Hence, the NSCT have better frequency characteristics than the CT. The two-level NSCT decomposition is shown in Fig. 1.
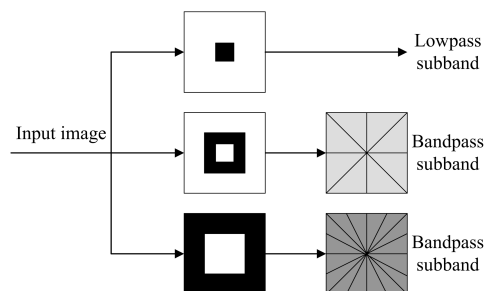
(a) NSFB structure that implements the NSCT

(b) Frequency partitioning obtained with the proposed structure

Fig. 1   Two level nonsubsampled contourlet transform decomposition

The core of the NSCT is the nonseparable two-channel NSFB. It is easier and more flexible to design the needed filter banks that lead to an NSCT with better frequency selectivity and regularity when compared to the corresponding CT. Based on mapping approach and ladder structure fast implementation, the NSCT frame elements are regular and symmetric, and the frame is close to a tight frame. The multiresolution decomposition of NSCT can be realized by nonsubsampled pyramid (NSP), which can reach the subband decomposition structure similar to LP. On j-th decomposition, the desired bandpass support of the low-pass is $[-\pi/2^j, \pi/2^j]^2$. And then the corresponding band-pass support of the high-pass is the complement set of the low-pass, that is $[-\pi/2^{j-1}, \pi/2^{j-1}]^2/[-\pi/2^j, \pi/2^j]^2$. The filters of subsequent scales can be acquired through upsampling that of the first stage, which gives the multiscale property without the need of additional filters design. From the computational complexity, one bandpass image is produced at each stage resulting in $J + 1$ redundancy. By contrast, the corresponding nonsubsampled wavelet transform (NSWT) produces three directional images at each stage and resulting in $3J + 1$ redundancy.

In this paper, the NSFB is built from a lowpass analysis filter $H_0(z)$ and $H_1(z) = 1 - H_0(z)$. The corresponding synthesis filter $G_0(z) = G_1(z) = 1$. The perfect reconstruction (PR) condition is given as

$$H_0(z)G_0(z) + H_1(z)G_1(z) = 1 \qquad (1)$$

In this way, the system is PR.

Since the NSCT is an oversampled redundancy representation, the PR condition is much easier to satisfy than that of critically sampled filter banks, and thus allows better filters to be designed.

The DFB of Bamberger and Smith[9] is constructed by combining critically sampled two-channel fan filter banks and resampling operations. The result is a tree-structured filter banks that split the two-dimensional frequency plane into directional wedges. In the design of the DFB, a shift-invariant directional expansion is not obtained because of existing downsamplers and upsamplers. A shift-invariant directional expansion can be obtained with a nonsampled DFB (NSDFB), which is constructed by eliminating the downsamplers and upsamplers in the DFB tree structure and upsampling the filters accordingly. The upsampling is based on the quincunx lattice, in which an image consisting of rectangular lattices is split into the round and square dot subsets. The adopted scale factor with rotated ability is as follows

$$A = \begin{pmatrix} 1 & 1 \\ 1 & -1 \end{pmatrix} \qquad (2)$$

The change of before and after quincunx interpolation is shown in Fig. 2, where a, b, c, and d are the four sampled points. The correlation of interpolation results before and after is given as
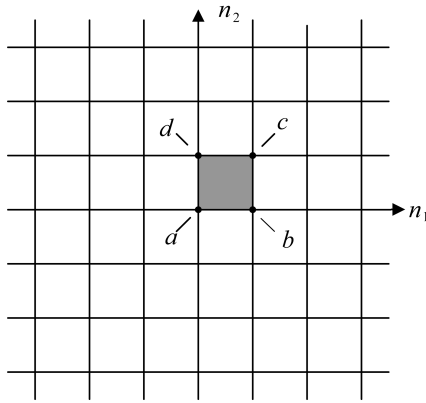
(a) The coordinate system before upsampling
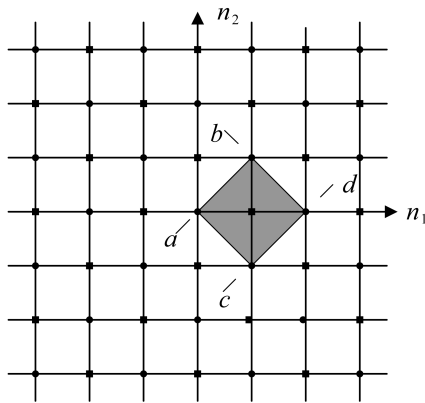
(b) The coordinate system after upsampling

Fig. 2 Quincunx upsample

$$y(n_1, n_2) =$$
$$\begin{cases} x(\dfrac{n_1 + n_2}{2}, \dfrac{n_1 - n_2}{2}), & \text{when } n_1, n_2 \text{ are even number} \\ 0, & \text{otherwise} \end{cases}$$
$$(3)$$

The corresponding z transform is denoted as

$$Y(z_1, z_2) = X(z_1 z_2, z_1 z_2^{-1}) \qquad (4)$$

The detail proof can be seen in [10].

If we give a two-level four-channel filter banks in the second level, the upsampled fan filter $U_j(z^Q)$, $j = 0, 1$, and when combined with the filters in the first level $U_k^{eq}(z) = U_i(z)U_j(z^Q)$ $(i = 0, 1)$, the four directional frequency decomposition is given. The synthesis filter bank is obtained similarly.

Just like the critically sampled DFB, all filter banks in the NSDFB tree structure are obtained from a single NSFB with fan filters. Moreover, each filter bank in the NSDFB tree has the same computational complexity as that of the building-block NSFB.

In order to simplify computation, the NSCT adopts mapping approach factor filters into ladder structures. The Euclidean algorithm enables us to factor the filters into the following ladder structures[11−12]:

$$\begin{pmatrix} H_0^{(1D)}(x) \\ H_1^{(1D)}(x) \end{pmatrix} = \prod_{i=0}^{N} \begin{pmatrix} 1 & 0 \\ P_i^{(1D)}(x) & 1 \end{pmatrix} \begin{pmatrix} 1 & Q_i^{(1D)}(x) \\ 0 & 1 \end{pmatrix} \begin{pmatrix} 1 \\ 0 \end{pmatrix} \qquad (5)$$

where $H_0^{(1D)}(x)$ and $H_1^{(1D)}(x)$ are adopted 1-D coprime prototype lowpass and highpass filters. The corresponding synthetic filters $G_0^{(1D)}(x)$ and $G_1^{(1D)}(x)$ satisfy the Bezout identity:

$$H_0^{(1D)}(x)G_0^{(1D)}(x) + H_1^{(1D)}(x)G_1^{(1D)}(x) = 0 \qquad (6)$$

Taking full consideration of the PR and anti-aliasing conditions in designing the filter banks, this paper can choose the needed prototype filters as

$$H_1^{(1D)}(x) = G_0^{(1D)}(-x)$$
$$G_1^{(1D)}(x) = H_0^{(1D)}(-x) \qquad (7)$$

In particular, we adopt the following prototype filter banks:

$$H_1^{(1D)}(x) = \frac{1}{2}(x+1)[\sqrt{2} + (1 - \sqrt{2})x]$$

$$G_1^{(1D)}(x) = \frac{1}{2}(x+1)[\sqrt{2} + (4 - 3\sqrt{2})x + (2\sqrt{2} - 3)x^2] \qquad (8)$$

2 High resolution and multispectral remote sensing image fusion based on LHS transform and nonsubsampled contourlet transform

In this section, an adaptive panchromatic and multispectral remote sensing image fusion technique is presented based on the NSCT and the LHS transform after analyzing

the basic principles of PAN image and MS image and fusion purpose. Here, we adopt an intensity (brightness) component addition method, that is, the detail information of the high-resolution PAN image is added to the corresponding intensity component of the low-resolution image's high frequency subbands to preserve some spectral information.

An image can be represented by RGB color system in computer. However, the RGB color system disagrees with the comprehensive and cognition habits of the human visual system. Human always recognize the color with three features, that is, intensity (I), hue (H), and saturation (S), called IHS system. I component is decided by the spectral main wave length and denotes the nature distinction. S component symbolizes the proportion of the main wave length of the intensity. I component means the brightness of the spectral. In the IHS space, spectral information is mostly reflected on the hue and the saturation. From the visual system, we can conclude that the intensity change has little effect on the spectral information and is easy to deal with.

For the fusion of the high-resolution and multispectral remote sensing images, the goal is ensuring the spectral information and adding the detail information of high spatial resolution, therefore, the fusion is even more adequate for treatment in IHS space.

IHS color space transform means the change of image from RGB space components to IHS spatial information I component and spectral information H and S components. However, the general IHS color system has the disadvantage that neglects two components when computing the brightness values. The IHS system results in that the brightness of pure color is the same as the achromatic color. Therefore, we adopt the LHS color system to solve the problem. The LHS color system generates the brightness with the value of 255 to achromatic color pixel and the value of 85 to pure color pixel[13].

The detailed process of the new fusion algorithm is as follows:

1) Perform polynomial interpolation to keep the edges of the linear landmark and make the PAN and SPOT images with the same sizes.

2) Transform the RGB representation of the multispectral image by LHS transformation into the intensity, hue, and saturation (L, H, S) components.

$$L = \frac{r + g + b}{3} \tag{9}$$

$$S = 1 - 3 \times \frac{\min(r, g, b)}{r + g + b} \tag{10}$$

$$H = \frac{\arccos(0.5 \times ((r - g) + (r - b)))}{\sqrt{(r - g)^2 + (r - b)(g - b)}} \tag{11}$$

The corresponding matrix expression is as follows

$$\begin{pmatrix} I \\ v_1 \\ v_2 \end{pmatrix} \begin{pmatrix} \frac{1}{3} & \frac{1}{3} & \frac{1}{3} \\ \frac{1}{\sqrt{6}} & \frac{1}{\sqrt{6}} & \frac{-2}{\sqrt{6}} \\ \frac{1}{\sqrt{2}} & \frac{-1}{\sqrt{2}} & 0 \end{pmatrix} \begin{pmatrix} R \\ G \\ B \end{pmatrix} \tag{12}$$

$$H = \tan^{-1}(\frac{v_1}{v_2}) \tag{13}$$

$$S = \sqrt{v_1^2 + v_2^2} \tag{14}$$

3) Apply histogram matching between the original panchromatic image and multispectral intensity component to get new panchromatic high-resolution (PAN HR) image and multispectral intensity (MSI) component image.

4) Decompose the matched MSI image and PAN HR image to get the NSCT decomposition coefficients.

5) Fuse the detail and approximate coefficients of the MSI and PAN HR according to (15) and (16), respectively.

$$Fuse_{low} = MSI_{low} \tag{15}$$

$$Fuse_{high} = \sum MSI_{details} + \sum PANHR_{details} \tag{16}$$

6) Apply the inverse NSCT transform to the fused detail and approximate coefficients to reconstruct the new intensity component I_{new}.

7) Perform the inverse LHS transform to the new intensity component, new I, together with the hue and saturation components, to obtain the fused RGB image.

$$\begin{pmatrix} R \\ G \\ B \end{pmatrix} \begin{pmatrix} 1 & \frac{1}{\sqrt{6}} & \frac{1}{\sqrt{2}} \\ 1 & \frac{1}{\sqrt{6}} & -\frac{1}{\sqrt{2}} \\ 1 & \frac{-2}{\sqrt{6}} & 0 \end{pmatrix} \begin{pmatrix} I_{new} \\ v_1 \\ v_2 \end{pmatrix} \tag{17}$$

3   Experiments and results

The test source images are the SPOT PAN image and LANDSAT TM 5, 4, 3 bands image of the same area. The TM image was acquired on February 17, 1993, and the SPOT PAN image was obtained on May 28, 1995. The two source images were after geometric adjustment and with the size of 256×256.

The fusion methods are traditional PCA and IHS, wavelet transform-based weighted fusion (WT-W), wavelet transform and LHS transform-based (WT-LHS), contourlet transform and LHS transform-based (CT-LHS), and non-subsampled contourlet transform and LHS transform-based (NSCT-LHS). Without loss of generality, the decomposition levels of the adopted transforms are all three. The WT adopts the 9-7 biorthogonal wavelet. The corresponding LP filter banks of CT and NSCT are all adopted 9-7 filter banks obtained from 9-7 1-D prototypes. And the DFB are adopted "pkva" ladder filters proposed by Phong et al.[14], which are with the decomposition 0, 3, 4 corresponding to the three levels of LP decomposition, respectively. The fusion results are shown in Fig. 3 (see next page).

From the human visual system, we can see that our fusion technique based on the NSCT-LHS can improve spatial resolution and at the same time hold spectral information well. Our intensity added fusion technique based on LHS transform is superior to classical PCA fusion method and IHS transform fusion method, and the WT-W fusion method. The fused image has more information of the source images, which is demonstrated in spatial resolution, definition, micro-detail difference, and contrast. The adaptive intensity component addition method preserves the whole spatial information, which has the advantage of

(a) SPOT image (b) TM image (c) PCA fusion image (d) IHS fusion image

(e) Wavelet weighted fusion image (f) Wavelet+LHS fusion image (g) Contourlet+LHS (h) Nonsubsampled contourlet+LHS
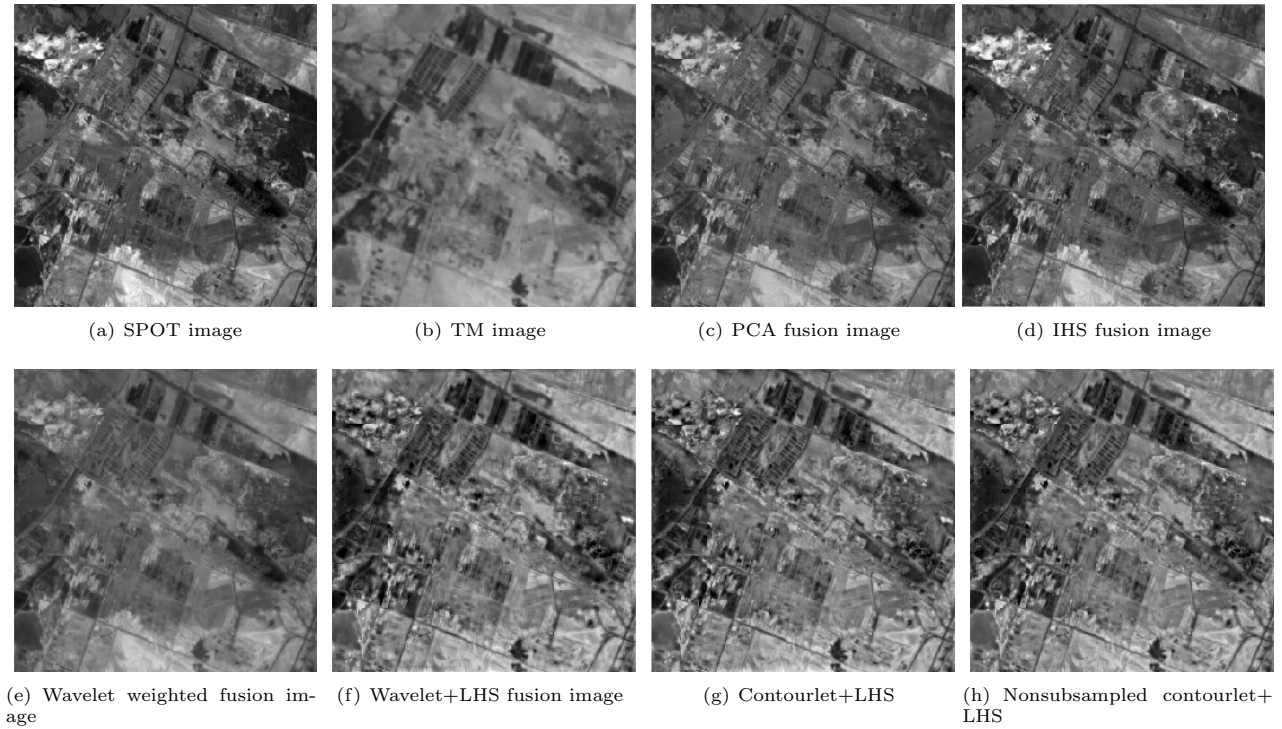
Fig. 3   Remote sensing image fusion based on NSCT and LHS transforms

the utilization of the detail information of the two source images. The fusion method only uses high-resolution information to adjust intensity component and better holds the multispectral information and texture information and introduces the high-resolution characteristic in multispectral image. Moreover, the fusion algorithm based on NSCT-LHS has more outstanding detail information than those based on WT-LHS and CT-LHS.

Subjective visual perception gives direct comparisons. However, it is easily influenced by visual psychological factors. The effect of image fusion should be based on subjective vision and objective quantitative evaluation criteria. For the remote sensing images, the desired standard image cannot be acquired. Then, the indexes such as root mean square error and peak value of signal to noise are unusable. In this paper, we adopt the following statistic indexes to performance, such as mean value, standard deviation, entropy, average gradient, correlation coefficient, spectrum distortion, weighted fusion quality index, and edge-dependent fusion quality index.

1) Mean value (MV): The MV is the gray mean value of the pixels in an image and the average brightness reflecting to human eye. Suppose the size of the image is M by N, and that $I(i, j)$ is the pixel in the image. Then the MV is defined as

$$MV = \frac{1}{MN} \sum_{i=0}^{N-1} \sum_{j=0}^{M-1} I(i, j) \qquad (18)$$

2) Standard deviation (STD): The variance of image reflects the dispersion degree between the gray values and the gray mean value. The STD is the square root of the variance. The larger the STD is, the more disperse the gray level. The definition of the STD is

$$STD = \sqrt{\frac{\sum_{i=0}^{N-1} \sum_{j=0}^{M-1} I(i, j)}{NM}} \qquad (19)$$

3) Information entropy (IE): The IE of the image is an important index to measure the abound degree of the image information. Based on the principle of Shannon information theory, the IE of the image is definition as

$$E = - \sum_{i=0}^{255} P_i \log_2 P_i \qquad (20)$$

where P_i is the ratio of the number of the pixels with gray value equal to i over the total number of the pixels. IE reflects the capacity of the information carried by images. The larger the IE is, the more information the image carries.

4) Average gradient (AG): AG is the index to reflect the expression ability of the little detail contrast and texture variation, and the definition of the image. The calculation formula is

$$g = \frac{1}{(M-1)(N-1)} \sum_{i=1}^{(M-1)(N-1)} \sqrt{\frac{(\frac{\partial f}{\partial x})^2 + (\frac{\partial f}{\partial y})^2}{2}} \qquad (21)$$

Generically, the larger g, the more the hierarchy, and the more definite the fused image.

5) Correlation coefficient (CC): The CC denotes the degree of correlation of two images. The more the CC close to 1, the higher the correlation degree is. The definition is denoted as

$$corr(\frac{A}{B}) = \frac{\sum\limits_{j=1}^{N}\sum\limits_{i=1}^{M}(x_{i,j}-\mu(A))(x'_{i,j}-\mu(B))}{\sqrt{\sum\limits_{j=1}^{N}\sum\limits_{i=1}^{M}(x_{i,j}-\mu(A))^2(x'_{i,j}-\mu(B))^2}} \qquad (22)$$

where A and B are two images, $x_{i,j}$ and $x'_{i,j}$ denote the pixels of A and B, respectively, $\mu(A)$ and $\mu(B)$ are the corresponding mean values of the two images.

6) Spectrum distortion (SD): SD means the distortion degree of a multispectral image and is defined as follows:

$$W = \frac{1}{M \times N}\sum\limits_{j=1}^{N}\sum\limits_{i=1}^{M}|I_f(i,j)-I(i,j)| \qquad (23)$$

where $I(i,j)$ and $I_f(i,j)$ are the pixels of the source and fused images, respectively. The larger value of W, the higher the distortion.

7) Bias index: This is an index of the deviation degree between fused image and low-resolution multispectral image:

$$Bias = \frac{1}{M \times N}\sum\limits_{j=1}^{N}\sum\limits_{i=1}^{M}\frac{|I_f(i,j)-I(i,j)|}{I(i,j)} \qquad (24)$$

8) Weighted fusion quality index (WFQI) and edge-dependent fusion quality index (EFQI)[15]: WFQI and EFQI are evaluation indexes without standard referrence image and consider some aspect of the human visual system. Suppose y'_A, y'_B, and y'_F are edge images of the source images y_A, y_A, and fused image y_F, respectively. WFQI is introduced to weight feature information of the fused images that come from source images. EFQI focuses on human visual system sensitivity to the edge information. The two measures have a dynamic range of $[-1, 1]$. The closer the value to 1, the higher the quality of the composite image is.

$$Q_{WFQI}(y_A, y_B, y_F) = \sum\limits_{\omega \in Q}c(\omega)(\rho_A(\omega)Q_0(y_A, y_F, |\omega))+$$
$$(1-\rho_A(\omega))Q_0(y_B, y_F, |\omega) \qquad (25)$$

$$Q_{EFQI}(y_A, y_B, y_F) = Q_{WFQI}(y_A, y_B, y_F)^{1-\alpha}\times$$
$$Q_{WFQI}(y'_A, y'_B, y'_F)^{\alpha} \qquad (26)$$

where $c(\omega) = C(\omega)/[\sum_{\omega \in Q}C(\omega')]$, and $C(\omega) = \max(\eta((y_A|\omega), \eta(y_B|\omega)))$ denotes the overall saliency of a window, $\rho_A(\omega) = \eta((y_A|\omega))/(\eta((y_A|\omega) + \eta(y_B|\omega))$, $(y_A|\omega)$ is some salient feature of image y_A in the window ω. In this paper, we select the energy as the salient feature and the size of the window is 3×3. Q is the summation of the total windows and Q_0 is the general image quality index. The parameter α in (26) expresses the contribution of the edges images compared to the original images, and its variation range is $[0, 1]$. In this paper, we select $\alpha = 0.2$. [9] adopted LOG operator to obtain the edge image. However, the LOG operator cannot provide the edge directional information and is sensitive to noise. Therefore, we select Canny operator to detects the edge information, which detects the edges by searching the local maximum of image gradient. Canny operator detects the strong edges and weak edges with two thresholds, respectively, where the thresholds are system automatic selection. Just when the weak edges and strong edges are jointed and the weak edges may be combined in the output. The Canny operator is not sensitive to noise and can detect the true weak edges.

From Table 1, we can see that the quantitative evaluation indexes are in accord with the visual effect. The fusion results based on our adaptive fusion technique are superior to the traditional PCA and IHS fusion methods, which embody the moderate brightness and the dispersion degree between the gray values, the larger entropy, the stronger correlation degree, the smaller spectrum distortion degree and bias deviation degree. From the whole effects, and by virtue of our proposed adaptive fusion technique, the non-subsampled contourlet transform-based fused results are better than those of the wavelet transform-based, and the contourlet transform-based, respectively, especially for the spectral holding. The better values are underlined.

The comparison of the histogram images of the R, G, B components of the TM multispectral image and the NSCT-based fusion image are shown in Fig. 4 (see next page), respectively.

From the comparison of the R, G, and B components histograms, we can conclude that the dynamic range of fused image is larger than that of the source image, that is, the fused image has more detail information and higher special resolution than that of the source image.

Table 1   Comparison of fusion results

Fusion metgods	MV	STD	IE	AG	CC	SD	$Bias$	Q_W	Q_E
Source image: TM	112.8229	47.6839	4.9623	9.4946	-	-	-	-	-
Source image: SPOT	92.4453	42.5459	5.0436	12.749	-	-	-	-	-
PCA fusion	94.0803	46.6214	5.0873	<u>18.7378</u>	0.5211	58.4023	0.5829	0.5373	<u>0.5133</u>
IHS fusion	92.4500	50.8016	5.2449	13.8455	0.6564	38.2370	0.3625	0.5195	0.5033
WT-weight fusion	102.8837	37.5430	4.9977	8.8577	0.8520	32.2293	0.2681	0.5157	0.4271
WT-LHS fusion	112.6562	<u>54.3067</u>	<u>5.3260</u>	16.2095	0.9171	14.7896	0.1390	0.5113	0.4392
CT-LHS fusion	112.6634	53.2326	5.3133	16.7984	0.9198	15.0153	0.1399	0.5194	0.4481
NACT-LHS fusion	<u>112.7205</u>	52.6581	5.3046	16.7634	<u>0.9268</u>	<u>14.2235</u>	<u>0.1329</u>	<u>0.5390</u>	0.4704

(a) R component of TM source image

(b) R component of NSCT-LHS fusion image

(c) G component of TM source image

(d) G component of NSCT-LHS fusion image

(e) B component of TM source image

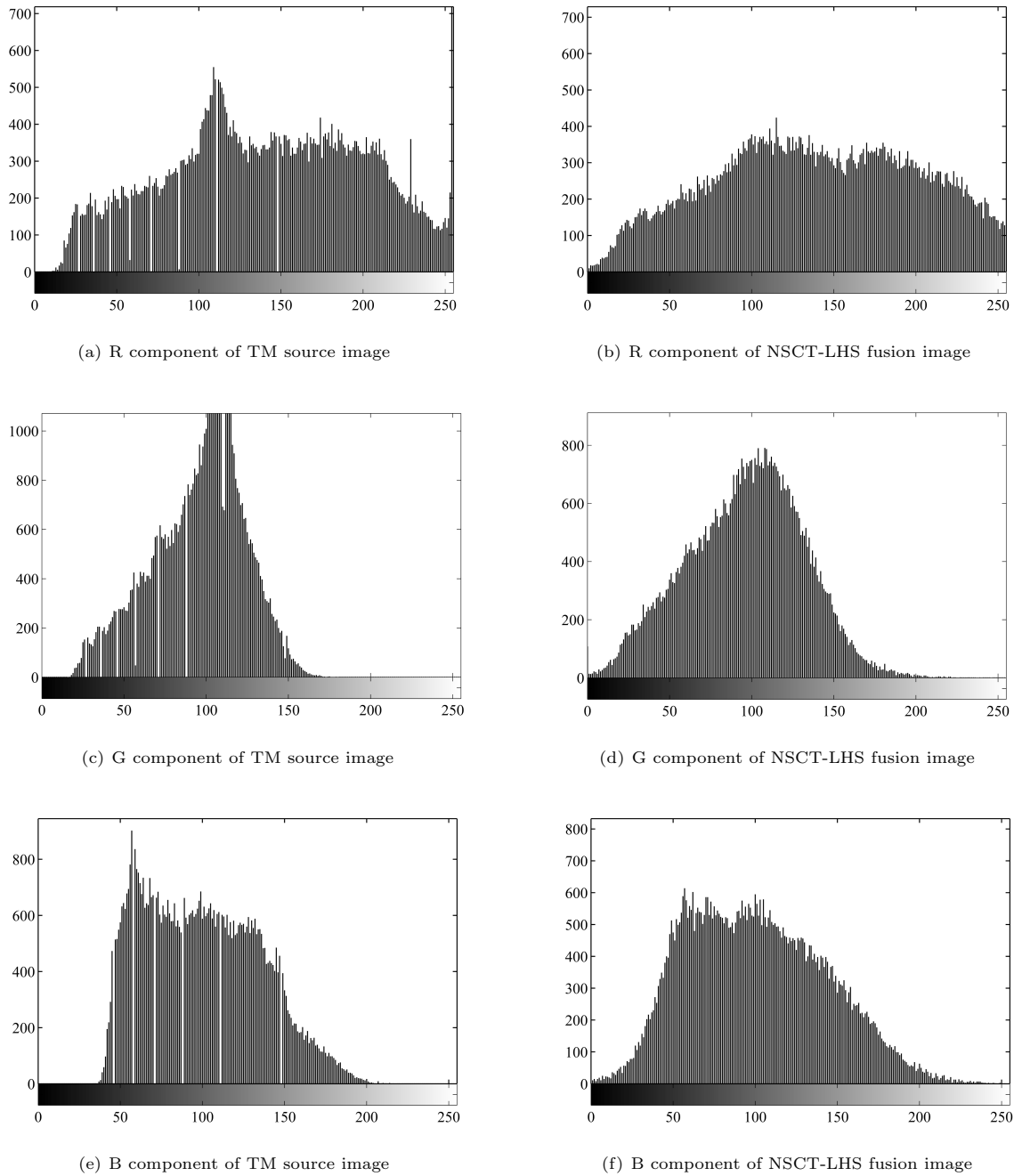
(f) B component of NSCT-LHS fusion image

Fig. 4　The R, G, and B components histograms of TM source image and the NSCT-LHS fusion image

4　Conclusions

A novel panchromatic high-resolution image and multispectral image fusion technique is proposed in this paper, which is based on nonsubsampled contourlet transform and LHS transform. We take full advantage of the nonsubsampled contourlet transform, including good multiresolution, shift-invariance, and multidirectional decomposition. And an intensity component addition technique is introduced into the NSCT domain to better improve the spatial resolution and hold the spectral information and texture information, simultaneously. Experiments show that the proposed fusion technique is more effective than other traditional fusion methods and has some improvements, especially for holding of spectral information, texture information, and contour information.

References

1 Rockinger O. Pixel-level fusion of image sequences using wavelet frames. In: Proceedings of Image Fusion and Shape Variability Techniques. Leeds, UK: Leeds University Press, 1996. 149−154

2 Gonzalez A M, Saleta J L, Catalan R G, Garcia R. Fusion of multispectral and panchromatic images using improved IHS and PCA mergers based on wavelet decomposi-

tion. *IEEE Transactions on Geoscience and Remote Sensing*, 2004, **42**(6): 1291−1299

3 Wang Z J, Ziou D, Armenakis C, Li D, Li Q G. A comparative analysis of image fusion methods. *IEEE Transactions on Geoscience and Remote Sensing*, 2005, **43**(6): 1391−1402

4 Nunez J, Otazu X, Fors O, Prades A, Pala V, Arbiol R. Multiresolution-based image fusion with additive wavelet decomposition. *IEEE Transactions on Geoscience and Remote Sensing*, 1999, **37**(3): 1204−1211

5 Do M N, Vetterli M. The contourlet transform: an efficient directional multiresolution image representation. *IEEE Transactions on Image Processing*, 2005, **14**(12): 2091−2106

6 Da Cunha A L, Zhou J P, Do M N. The nonsubsampled contourlet transform: theory, design and applications. *IEEE Transactions on Image Processing*, 2006, **15**(10): 3089−3101

7 Simoncelli E P, Freeman W T, Adelson E H, Heeger D J. Shiftable multiscale transforms. *IEEE Transactions on Information Theory*, 1992, **38**(2): 587−607

8 Zhou J P, Da Cunha A L, Do M N. Nonsubsampled contourlet transform: construction and application in enhancement. In: Proceedings of IEEE International Conference on Image Processing. Genoa, Italy: IEEE, 2005. 469−472

9 Bamberger R H, Smith M J T. A filter bank for the directional decomposition of images: theory and design. *IEEE Transactions on Signal Process*, 1992, **40**(4): 882−893

10 Yang Fu-Sheng. *Project Analysis and Application of Wavelet Transform*. Beijing: Scientific Press, 1999. 121−126 (in Chinese)

11 Vaidyanathan P P. *Multirate Systems and Filter Banks*. New Jersey, USA: Prentice-Hall, 1993

12 Kovacevic J, Vetterli M. Nonseparable multidimensional perfect reconstruction filter banks and wavelet bases for $\mathbf{R}^n$. *IEEE Transactions on Information Theory*, 1992, **38**(2): 533−555

13 Tan Zheng, Bao Fu-Min, Li Ai-Guo, Yang Bo, Gong Ya-Ge. *Digital Image Fusion*. Xi′an: Xi′an Jiaotong University Press, 2004 (in Chinese)

14 Phoong S M, Kim C W, Vaidyanathan P P. A new class of two-channel biorthogonal filter banks and wavelet bases. *IEEE Transactions on Signal Processing*, 1995, **43**(3): 649−661

15 Piella G. New quality measures for image fusion [Online], available: http://www.fusion2004.foi.se/papers/IF04-0542.pdf, 2004

YANG Xiao-Hui   Received her master degree from College of Mathematics and Information Science of Henan University in 2004. She is a Ph. D. candidate in Institute of Intelligent Information Processing at Xidian University. Her research interest covers multiresolution geometry analysis and the applications in image processing, and filter design. Corresponding author of this paper. E-mail: xhyang_lc@163.com

JIAO Li-Cheng   Professor in Institute of Intelligent Information Processing at Xidian University. His research interest covers nonlinear science, intelligent information processing, and multiresolution geometry analysis.
E-mail: lchjiao@mail.xidian.edu.cn